



Supporting Online Material for

Plastic Deformation of MgGeO₃ Post-Perovskite at Lower Mantle Pressures

Sébastien Merkel,* Atsushi Kubo, Lowell Miyagi, Sergio Speziale, Thomas S. Duffy,
Ho-kwang Mao, Hans-Rudolf Wenk

*To whom correspondence should be addressed. E-mail: smerkel@berkeley.edu

Published 3 February, *Science* **311**, 644 (2006)
DOI: 10.1126/science.1121808

This PDF file includes:

Materials and Methods
Figs. S1 to S4
Tables S1 and S2
References

Supporting Online Material

1 Experimental details

High-pressures and high temperatures were generated in a laser heated diamond anvil cell with large openings to allow radial diffraction. The sample was loaded in an 80 μm diameter hole in a beryllium gasket preindented to 20 μm thickness and compressed with 300 μm bevel, 150 μm inner culet, diamond anvils. Pressure was determined using the equation of state of platinum (*S1*). The lattice parameter of Pt was obtained from the 111, 220 and 311 diffraction lines, corrected for the effect of non-hydrostatic stress. Because of uncertainties in the equation of state of Pt, effects of non-hydrostatic stress, and possible stress gradients in the sample, we estimate that the total uncertainty in pressure is on the order of ± 5 GPa. Diffraction patterns were collected in radial geometry (Fig. S2) with a Mar345 image plate detector (3450 pixels diameter) and a monochromatic incoming x-ray beam ($\lambda = 0.4224 \text{ \AA}$). Sample to detector distance and detector non-orthogonality were determined using a CeO_2 standard prior to the experiment. Laser heating was performed by focusing a Nd:YLF laser ($\lambda = 1053 \text{ nm}$) to a 30 μm spot and temperature was measured by thermal radiance spectrometry. In order to improve the signal to noise ratio and overcome saturation on the image plate, the diffraction patterns were also collected as multiple exposures (up to 20, with 30 seconds accumulation for each spectrum) and summed before processing.

2 Data processing

The spectrum contains diffraction lines from pPv and Pt in addition to Be and BeO from the gasket. Be and BeO peaks are very intense compared to those of the sample, however, many peaks of MgGeO₃-pPv do not overlap with Be or BeO and can be fully analyzed.

The individual peak fitting used the 020, 002, 022, 110, 112, and 130 diffraction lines of MgGeO₃-pPv to calculate the orientation distribution function with the software Beartex (*S2*) and stress using lattice strain theory (*S3*) (Figs. S3 and S4). The same images were also analyzed with the Rietveld method implemented in the code MAUD (*S4*) using the continuous range 5.5°-10.2° in 2θ . In the absence of information about the shear modulus of MgGeO₃-pPv, we assumed a constant value of 300 GPa for calculating the deviatoric stress component t (*S5*).

3 Calculation of seismic velocities

Bulk elastic constants of the polycrystal were calculated using the software package Beartex (*S2*), using the single crystal elastic moduli at 135 GPa and 4000 K of (*17*) and the ODF obtained from VPSC simulations after a deformation in simple shear up to a strain of 0.5. From the aggregate elastic tensor we then calculated and plotted seismic velocities in different directions using the petrophysics software package of D. Mainprice (*S6*).

References and Notes

- S1. N. C. Holmes, J. A. Moriarty, G. R. Gathers, W. J. Nellis, *J. Appl. Phys.* **66**, 2962 (1989).
- S2. H. R. Wenk, S. Matthies, J. Donovan, D. Chateigner, *J. Appl. Cryst.* **31**, 262 (1998).
- S3. A. K. Singh, C. Balasingh, H. K. Mao, R. J. Hemley, J. Shu, *J. Appl. Phys.* **83**, 7567 (1998).

- S4. L. Lutterotti, S. Matthies, H. R. Wenk, *Proceeding of the Twelfth International Conference on Textures of Materials (ICOTOM-12)* (1999), p. 1599.
- S5. The bulk modulus MgGeO₃-pPv is 5-10% lower than that of MgSiO₃-pPv (Kubo et al, Shieh et al, unpub. data). From ab initio calculation, we also have $G = 328$ GPa at 120 GPa for MgSiO₃-pPv (Ref. 2). Therefore it is reasonable to assume that $G \approx 300$ GPa in the 105-130 GPa pressure range for MgGeO₃-pPv.
- S6. D. Mainprice, *Computers & Geosciences* **16**, 385 (1990).

4 Tables

Table S1: Pressure, temperature, and time path of the experiment along with the deviatoric stress t , unit cell parameters, a , b , and c , and texture indices iF_2 and fF_2 measured in MgGeO₃-pPv using the individual peak fitting and full profile refinement Rietveld techniques, respectively.

Name	Action	Time	P (GPa)	t (GPa)	a (Å)	b (Å)	c (Å)	iF_2	fF_2
P08b	Heated to 1600K	0h	104(5)	3.6(1)	2.581(1)	8.336(5)	6.363(3)	1.29	1.34
P09	Increased pressure	3h	110(5)	5.1(1)	2.572(1)	8.309(4)	6.343(3)	1.32	1.35
P10	Increased pressure	5h	124(5)	8.2(1)	2.557(1)	8.254(3)	6.309(2)	1.30	1.46
P11	Waited	20h	126(5)	8.9(1)	2.554(1)	8.246(2)	6.302(1)	1.33	1.46
P11b	Heated to 1600K	23h	128(5)	8.0(1)	2.551(1)	8.225(2)	6.294(1)	1.32	1.50
P12	Waited	41h	130(5)	8.9(1)	2.549(1)	8.217(6)	6.289(4)	1.31	1.55

Table S2: Slip systems and critical resolved shear stress (CRSS) ratios used for VPSC modeling in compression for model 1, 2, 3, and 4 that favor slip on (100), (010), (001), and both (100) and (110), respectively. Average slip systems activities are calculated after 20% compressive strain.

	(100)[001]		(100)[010]		(110)[$\bar{1}10$]		(010)[100]		(010)[001]		(001)[100]		(001)[010]	
	CRSS	Act.	CRSS	Act.	CRSS	Act.	CRSS	Act.	CRSS	Act.	CRSS	Act.	CRSS	Act.
1	2	38%	1	38%	10	10%	10	2%	10	2%	10	5%	10	5%
2	10	4%	10	0%	10	6%	1	41%	1	41%	10	4%	10	4%
3	10	0%	10	2%	10	7%	10	2%	10	2%	1	43%	1	43%
4	2	23%	1	8%	1	57%	5	1%	5	1%	5	5%	5	5%

5 Figures

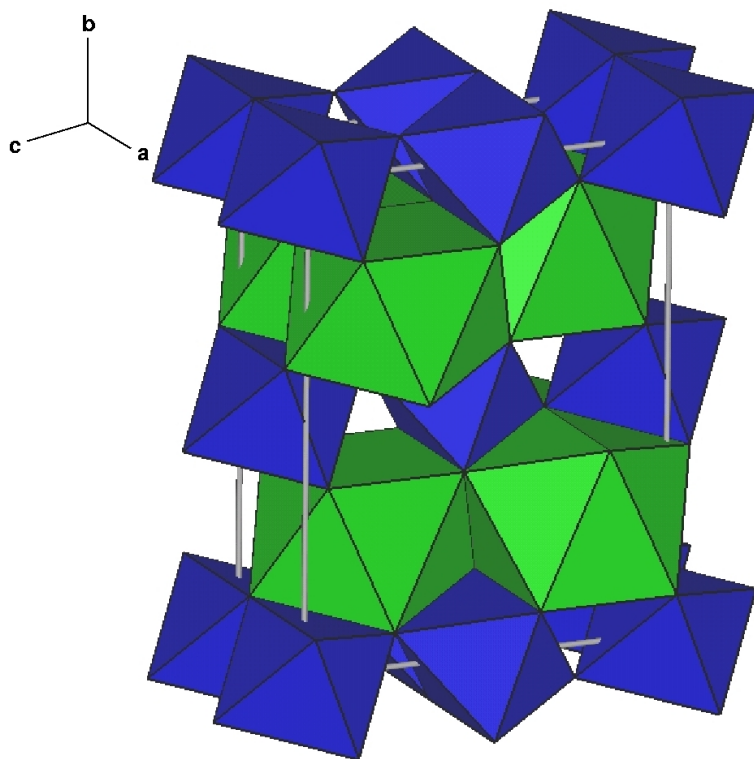


Fig. S1: Crystallographic structure of the post-perovskite phase of MgGeO₃ (after (23)). GeO₆ and MgO₆ polyhedra are shown in blue and green, respectively.

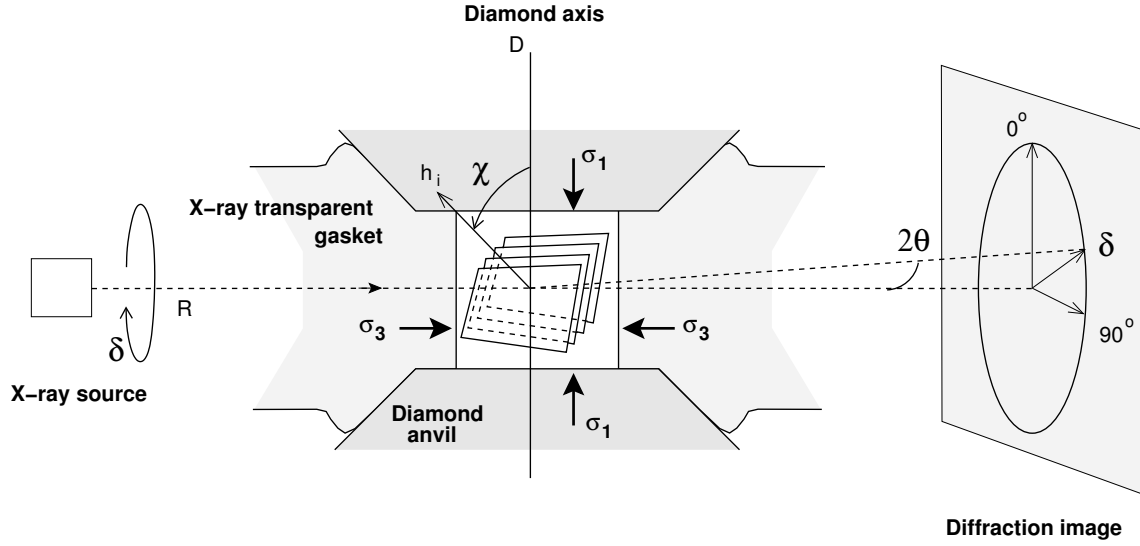


Fig. S2: Schematic of the experiment. The polycrystalline sample is confined under non-hydrostatic stress conditions between the two diamond anvils. σ_1 is the axial stress imposed by the diamonds and σ_3 the radial stress imposed by the gasket. A monochromatic x-ray beam is sent through the gasket and the data collected on an imaging plate orthogonal to the incoming beam. The position of the diffraction lines and intensity of diffraction are analyzed as a function of the azimuthal angle δ from which we calculate the angle χ between the normal to the diffracting plane h_i and the compression direction.

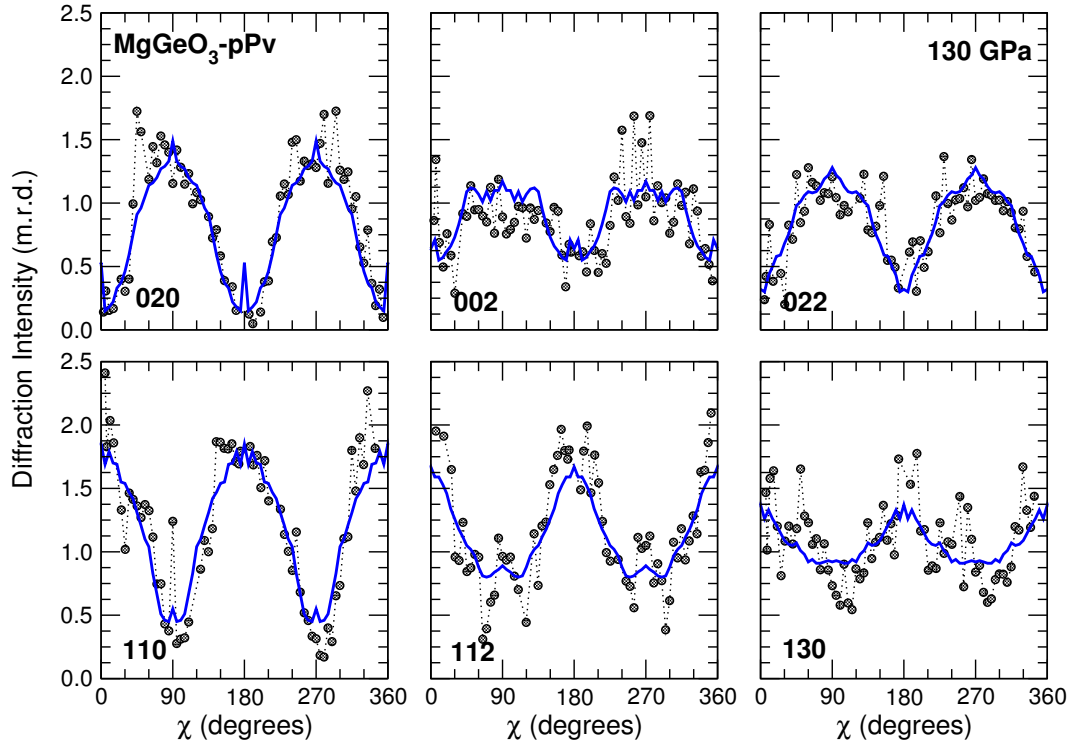


Fig. S3: Measured diffraction intensities using the single peak fitting techniques (closed circles) and those recalculated from the orientation distribution function (solid blue lines) as a function of the pole distance χ for the peaks 020, 002, 022, 110, 112, and 130 of $\text{MgGeO}_3\text{-pPv}$ at 130 GPa. Experimental intensities have been scaled to match those recalculated from the ODF, expressed in m.r.d.

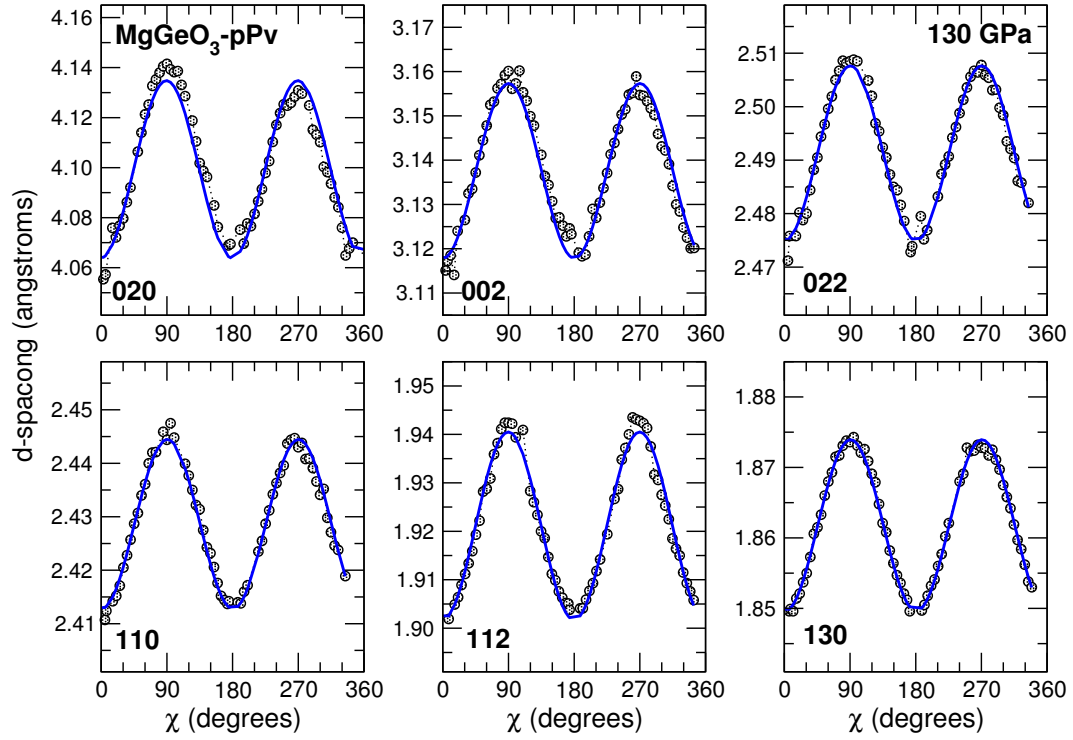


Fig. S4: Measured d-spacing using the single peak fitting techniques (closed circles) and models used for lattice strain analysis (solid blue lines) as a function of the pole distance χ for the peaks 020, 002, 022, 110, 112, and 130 of MgGeO₃-pPv at 130 GPa.